# Gas-Phase Reactions of Nitronium Ions with Acetylene and Ethylene: An Experimental and Theoretical Study

**Fernando Bernardi,*[b] Fulvio Cacace,[a] Giulia de Petris,*[a] Federico Pepi,[a] Ivan Rossi,[b] and Anna Troiani[a]**

**Abstract:** A comparative study of the gas-phase reactions of $NO_2^+$ with acetylene and ethylene was performed by using FT-ICR, MIKE, CAD, and $N_tR$/CA mass spectrometric techniques, in conjunction with ab initio calculations at the MP2/6–31+G* level of theory. Both reactions proceed according to the same mechanism, that is, 1,3-dipolar cycloaddition, but yield products of different stability. The $C_2H_2NO_2^+$ adduct from acetylene has an aromatic character and hence is highly stabilized with respect to the $C_2H_4NO_2^+$ adduct from ethylene. Both cycloadducts tend to isomerize into *O*-nitroso derivatives, that is, nitrosated ketene and nitrosated acetaldehyde, which represent the thermodynamically most stable products from the addition of $NO_2^+$ to acetylene and ethylene, respectively. As prototypal examples of the reactivity of free nitronium ions with most simple π systems, the reactions investigated are useful starting points to model the mechanism of aromatic nitration.

**Keywords:** ab initio calculations · alkynes · cycloadditions · gas-phase chemistry · mass spectrometry

## Introduction

In this paper, we report the results obtained in a combined experimental and theoretical study of the addition of nitronium ions to acetylene [Eq. (1)].

$$NO_2^+ + C_2H_2 \rightarrow [C_2H_2NO_2]^+ \quad (1)$$

For comparison, we discuss also the results obtained in a similar study of the reaction of nitronium ions with ethylene [Eq. (2)].

$$NO_2^+ + C_2H_4 \rightarrow [C_2H_4NO_2]^+ \quad (2)$$

These two processes represent prototypal examples of the electrophilic nitration of very simple π systems and a useful starting point to model electrophilic aromatic nitration, a reaction that has received great attention,[1–6] but whose mechanism has not been completely clarified yet. This work aims to bring about a detailed understanding of the two gas-phase reactions in Equations (1) and (2) through the combined application of experimental techniques and a detailed ab initio study at the MP2/6–31+G* level of theory. In particular, we report new theoretical and experimental results for the reaction in Equation (1), whereas for the reaction in Equation (2) we use both earlier experimental and theoretical results[7, 8] and new results that allow us to perform a more comprehensive comparative analysis of the two reactions. We have found that the two reactions are mechanistically very similar and that they proceed mainly according to a 1,3-dipolar-type addition. This reaction leads to the formation of two structurally related end products, nitrosated ketene from the reaction in Equation (1) and nitrosated acetaldehyde from the reaction in Equation (2).

[a] Prof. G. de Petris, Prof. F. Cacace, Dr. F. Pepi, Dr. A. Troiani
Dipartimento di Studi di Chimica e Tecnologia
delle Sostanze Biologicamente Attive
Università di Roma 'La Sapienza'
P. le Aldo Moro 5, 00185 Roma (Italy)
Fax: (+39) 06-4991-3602
E-mail: depetris@axrma.uniroma1.it

[b] Prof. F. Bernardi, Dr. I. Rossi
Dipartimento di Chimica'G. Ciamician'
Università di Bologna
Via Selmi 2, 40126 Bologna (Italy)
Fax: (+39) 051-259456

## Experimental Section

**Materials**: The gases were research grade products with a stated purity of >99.95 mol% (except NO, $NO_2$, and $C_2H_2$ >99.5 mol%). They were obtained from commercial sources and used without further purification. Ketene was obtained according to an established procedure,[9] whereas all other chemicals were research grade products from Aldrich Chemical Company.

**Instruments**: A model 47e APEX FT-ICR mass spectrometer (Bruker Spectrospin) was used, which was equipped with an external chemical ionization (CI)/EI ion source, a cylindrical "infinity" cell,[10] and a pulsed valve. The pressure was measured with a Bayard–Alpert ionization gauge,

  0947-6539/00/0603-0537 $ 17.50+.50/0 

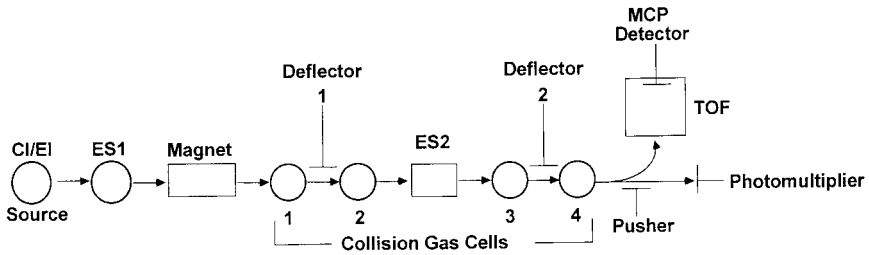


Figure 1. Schematic diagram of the apparatus for MIKE, CAD, and $N_f$R/CA mass spectrometry (see text).

whose readings were corrected by a standard procedure[11] according to the different sensitivities to the gases employed. The mass-analyzed ion kinetic energy (MIKE) and collisionally-activated dissociation (CAD) spectra were recorded by utilizing a version of the ZAB Spec oa-TOF spectrometer (Micromass), which is schematically illustrated in Figure 1. The ions from the EI, or the CI ion source entered the first electrostatic sector (ES1) and were mass selected by the magnet before they entered the first pair of collision cells, to which different gases can be admitted through individual metering valves. In the cells, any desired voltage with respect to ground could be selected, and the charged species from the first cell were prevented from entering the second one by the first deflecting electrode. Next, the ions were analyzed by the ES2 and they entered the second pair of gas collision cells before they reached the photomultiplier detector. If desired, application of a proper potential to a steering electrode, the "pusher", allowed the introduction of ions into the orthogonal TOF spectrometer, which was equipped with a micro channel plate (MCP) detector.

**Procedure: FT-ICR experiments**: The ions produced in the external source were transferred into the resonance cell and isolated by the usual procedure by using the "soft" ejection of all unwanted ions by low-intensity RF "shots". In this process, care was taken to prevent appreciable excitation of the species of interest. When required, the isolated ions were thermalized by collision with Ar, which was temporarily admitted into the cell by means of the pulsed valve for a period of 20 ms to a peak pressure of approximately $10^{-5}$ Torr.[12] After removal of Ar, the ions were allowed to react with the neutral reagent, which was continuously admitted into the cell and reached a stationary pressure of $10^{-8}$ to $10^{-7}$ Torr.

**MIKE and CAD spectrometry**: The MIKE spectra were recorded according to the standard procedure, which examines the metastable transitions in the third field-free region of the ZAB Spec oa-TOF spectrometer. The CAD spectra were recorded in two ways. The first (high-energy) approach utilized the second collision cell, where mass-selected ions were allowed to collide with the target gas (He). The pressure of the helium was adjusted in such a way as to reduce the original intensity of the ion beam by approximately 30%. In these experiments, the collision energy was 8 kV (laboratory frame), and the fragments analyzed by ES2 were detected by the photomultiplier. The second (low-energy) approach utilized the third collision gas cell. The voltage of the cell was set to 90% of the source voltage, so that the laboratory-frame collision energy was only 10% of the main acceleration voltage.

**Neutral fragments reionization/collisional activation ($N_f$R/CA) mass spectrometry**: This method was a new version of the well established $N_f$R technique,[13, 14] where the observed spectrum represented the *superimposition* of the individual collision-induced dissociative ionization (CIDI) spectra[15] of all the neutral fragments from the collision-activated dissociation of the precursor ion under study. In our experiments, mass-selected ions underwent high-energy (8 kV, laboratory frame) CAD in the collision gas cell **1**, as in the standard CAD spectrometry. The charged fragments and the undissociated parent ions were removed by applying a potential of 1 kV to deflector **1**, whereas the neutral fragments entered collision cell **2**, which contained the reionization gas ($O_2$). The charged species of interest were mass selected by scanning ES2 and driven into the collision cell **3** with He as the target gas, so that the CAD spectra of the ionic species from the reionization of *each* neutral fragment could be recorded *separately* by utilizing the TOF spectrometer. In certain cases, it was necessary to compare the $N_f$R/CA spectra with the CAD spectra of the molecular ions obtained in the EI source from model molecules. In these cases, the CAD spectra were recorded using the collision gas cell **3**. The main accelerating voltage was chosen so that the molecular ion could be transmitted from the EI source at exactly the same ES2 potential as that required for transmittance of the re-ionized neutral fragments in the $N_f$R/CA experiments.

## Results

### Acetylene nitration

*FT-ICR spectrometry*: $NO_2^+$ ions generated in the external ion source from nitrogen dioxide by charge exchange with $Xe^+$ were found to react with acetylene in two different ways; the way in which they react depends on their internal energy content. If $NO_2^+$ ions thermalized by collision with Ar are used,[12] only the formation of $NO^+$ is observed [Eq. (3)].

$$NO_2^+ + C_2H_2 \rightarrow NO^+ + C_2H_2O \quad (3)$$

If the thermalization procedure is omitted, the process in Equation (3) is accompanied by the reaction in Equation (4).

$$(NO_2^+)_{exc} + C_2H_2 \rightarrow C_2H_2O^{\bullet +} + NO \quad (4)$$

This reaction yields $C_2H_2O^{\bullet +}$ ions, which were positively identified by accurate mass measurements. It should be noted that the reaction in Equation (4) is energetically less favorable than that in Equation (3) owing to the higher ionization potential of $CH_2CO$ with respect to NO. This accounts for its occurrence only when excited $NO_2^+$ ions are used. As expected, no $C_2H_2NO_2^+$ adducts were observed at the low pressures, $10^{-8}$ to $10^{-7}$ Torr, which are typical of FT-ICR experiments. Nevertheless, evidence for a transient complex is provided by the O atom transfer from $NO_2^+$ to $C_2H_2$ indicated indirectly by the ionic product from the reaction in Equation (3) and directly by that from the reaction in Equation (4). The most reasonable explanation of the above results is that addition of $NO_2^+$ to acetylene is highly exothermic and yields an excited adduct that cannot escape dissociation. This is the result of the very low efficiency of collisional deactivation in FT-ICR experiments.

*Chemical ionization experiments*: The experiments are based on the FT-ICR results; the reaction in Equation (1) was performed in the CI source of the ZAB Spec oa-TOF spectrometer. The higher operating pressure of the spectrometer (up to several tenths of a Torr) was expected to ensure a much more efficient collisional stabilization of the excited $C_2H_2NO_2^+$ adduct. In actual fact, no detectable amounts of this ion were obtained, and the only processes promoted by the $NO_2$/CI of acetylene are again those given in Equations (3) and (4). This suggests that direct nitration of $C_2H_2$ by $NO_2^+$ is too exothermic to allow survival of $C_2H_2NO_2^+$ for the time required for its detection, and a milder route of formation is needed [Eq. (5)].

$$HNO_3NO_2^+ + C_2H_2 \rightarrow C_2H_2NO_2^+(\mathbf{A}) + HNO_3 \quad (5)$$



0947-6539/00/0603-0538 $ 17.50+.50/0 *Chem. Eur. J.* **2000**, *6*, No. 3

In this reaction, the free nitronium ion is replaced by its complex with nitric acid, prepared from $N_2O_5$ protonation and characterized as a $HNO_3$–$NO_2^+$ adduct with a binding energy (BE) of 18.3 kcal mol$^{-1}$.[16] From the thermochemical standpoint, the reaction in Equation (5) can be considered as a two-step process; the first step is the endothermic dissociation of the complex that yields free $NO_2^+$, which subsequently adds to acetylene. Hence, the reaction in Equation (5) is less exothermic than that in Equation (1) by 18.3 kcal mol$^{-1}$. Furthermore, the energy released is divided between the products, $C_2H_2NO_2^+$ and $HNO_3$. In fact, the reaction in Equation (5) proved to be a viable route to $C_2H_2NO_2^+$ and yielded significant intensities of the adduct **A** together with $NO^+$ and $C_2H_2O^{\bullet+}$.

*Structural studies*: The products from the reactions in Equations (4) and (5) were examined by structurally diagnostic techniques that included MIKE, CAD, and $N_f$R/CA mass spectrometry in the ZAB Spec oa-TOF instrument. The results for the various species of interest are illustrated in the following paragraphs.

*$C_2H_2NO_2^+$ ions*: The structural features of the ionic population (**A**) from the reaction in Equation (5) were compared with those of model ions of $H_2C$–C–O–$NO^+$ structure (population **B**) from the reaction in Equation (6).

$$CH_2{=}CO + NO^+ \rightarrow C_2H_2NO_2^+ \ (\mathbf{B}) \qquad (6)$$

This reaction involved NO/CI of ketene. The MIKE spectra results in Table 1 are appreciably different in that, as

Table 1. MIKE spectra of $C_2H_2NO_2^+$ ions from different sources.

| Fragment *m/z* | Relative intensity[a] Ions **A**[b] | Ions **B**[c] |
|---|---|---|
| 30 | 100 | 100 |
| 42 | 76 | – |
| 46 | 12 | – |

[a] Standard deviation ±10%. [b] From the reaction in Equation (5). [c] From the reaction in Equation (6).

expected, the only fragment from the model ions **B** is $NO^+$ (*m/z* 30), whereas ions **A** from the nitration of $C_2H_2$ undergo significant metastable transitions and give, in addition, $C_2H_2O^{\bullet+}$ (*m/z* 42) and $NO_2^+$ (*m/z* 46) fragments.

The CAD spectra of populations **A** and **B**, compared in Table 2, are particularly significant in that collision-activated dissociation is expected to provide a more reliable picture of the structure of the stable ionic population assayed.[15]

A comparison of the two spectra shows that there are considerable and structurally diagnostic differences; that is, the major fragments from model ion **B**, $NO^+$ and $C_2H_2O^{\bullet+}$, are consistent with its expected $H_2C$–CO–$NO^+$ structure, whereas the major fragment from population **A** is a nitronium ion (*m/z* 46), which suggests the presence of a strongly bonded O–N–O moiety within the $C_2H_2NO_2^+$ adduct from the nitration of acetylene. Nevertheless, the presence in the ionic population **A** of a minor fraction of ions with the

Table 2. High-energy CAD spectra of $C_2H_2NO_2^+$ ions from different sources.

| Fragment *m/z* | Relative intensity[a] Ions **A** | Ions **B** |
|---|---|---|
| 14 | – | 3 |
| 25 | 2 | – |
| 26 | 16 | – |
| 28 | – | 7 |
| 30 | 10 | 100 |
| 41 | – | 10 |
| 42 | 3 | 60 |
| 44 | – | 6 |
| 46 | 100 | – |

[a] Standard deviation ±10%

$H_2C$–C–O–NO structure is suggested by the low, but easily detectable, intensity of the $NO^+$ and $C_2H_2O^{\bullet+}$ fragments.

*$C_2H_2O^{\bullet+}$ ions*: As previously mentioned, formation of these ions was observed in different experiments, namely those that involve the reaction of $HNO_3NO_2^+$ with $C_2H_2$ ($CH_4/N_2O_5$ CI of $C_2H_2$) and the reaction of $NO_2^+$ with $C_2H_2$ (FT-ICR and $NO_2$/CI of $C_2H_2$). The $C_2H_2O^{\bullet+}$ ions from the latter source were analyzed by CAD spectrometry, and their spectrum was compared with that of $C_2H_2O^{\bullet+}$ model ions formed by EI of ketene. The spectra are indistinguishable; this suggests the $H_2C{=}CO^{\bullet+}$ structure for the charged product from the reaction in Equation (4). To make the assignment rigorous, it would be necessary to demonstrate that isomeric $C_2H_2O^{\bullet+}$ ions can be discriminated by CAD spectrometry.

**Ethylene nitration**: It is of interest to compare the results for the nitration of acetylene with those obtained in a recent study[8] of the ethylene nitration by free nitronium ions [Eq. (2)] and by protonated methyl nitrate [Eq. (7)].

$$C_2H_4 + NO_2^+ \rightarrow C_2H_4NO_2^+ \ (\mathbf{C}) \qquad (2)$$

$$C_2H_4 + CH_3OHNO_2^+ \rightarrow C_2H_4NO_2^+ \ (\mathbf{D}) + CH_3OH \qquad (7)$$

The CAD spectra of **C** and **D** were compared with those of model ions from the nitrosation of oxirane [Eq. (8)] and of acetaldehyde [Eq. (9)].

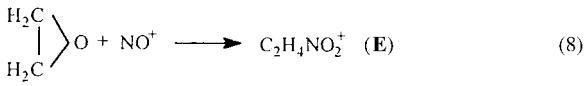


(8)

$$CH_3CHO + NO^+ \rightarrow C_2H_4NO_2^+ \ (\mathbf{F}) \qquad (9)$$

As previously reported in detail,[8] the CAD spectra of populations **C**, **E**, and **F** were found to be equal, but different from the spectrum of population **D** (see below); this led to the assignment of the *O*-nitrosated structure to the adduct from the nitration in Equation (2). However, it proved impossible to discriminate between ions **E** and **F**, namely to ascertain whether the product **C**, from the direct nitration of ethylene, had the nitrosated oxirane or the nitrosated acetaldehyde structure.[8] In order to clarify this point, we used the structurally diagnostic $N_f$R/CA technique in the present study.

*$N_fR/CA$ spectrometry of $C_2H_4NO_2^+$ ions*: The CAD spectra of the ionic populations **C**, **E**, and **F** display an intense $NO^+$ fragment, whose neutral counterpart(s), that is, the $C_2H_4O$ species, were reionized to give $C_2H_4O^+$ ions, which were mass selected, and their CAD spectra were recorded. Furthermore, model $C_2H_4O^+$ ions were obtained by EI ionization of oxirane (ions **G**) and of acetaldehyde (ions **H**), and their CAD spectra were compared with the $N_fR/CA$ spectra of $C_2H_4O$ from adducts **E**, **F**, and **C** (Table 3). The results show that the

Table 3. CAD spectra of model ions **G** and **H** from the EI of oxirane and acetaldehyde, and $N_fR/CA$ spectra of the $C_2H_4O$ neutral fragment from ions **C**, **E**, and **F** from the reactions in Equations (2), (8), and (9).

| *m/z* | Relative intensity[a] | | | | |
|---|---|---|---|---|---|
| | CAD | | $N_fR/CA$ | | |
| | **G** | **H** | **C** | **E** | **F** |
| 43 | 4.0 | 41.6 | 45.6 | 13.3 | 53.6 |
| 29 | 60.9 | 30.0 | 41.0 | 64.5 | 32.4 |
| 15 | 15.0 | 22.1 | 10.9 | 12.2 | 11.7 |
| 14 | 20.1 | 6.3 | 2.5 | 10.0 | 2.3 |

[a] Percentage of the sum of the intensities of the fragments. Standard deviation ±10%.

$C_2H_4O$ neutral fragment from the fragmentation of the model nitrosated adducts **E** and **F** is reminiscent of the structure of the $C_2H_4O$ neutral species utilized for their preparation, that is, oxirane and acetaldehyde, respectively.[17] Based on these findings, the $N_fR/CA$ spectrum of the neutral $C_2H_4O$ fragment from **C** (Table 3) allows one to assign the $CH_3CHONO^+$ structure to the latter species rather than the structure illustrated below. The reaction in Equation (7) promoted by the $CH_3OHNO_2^+$ complex has been calculated to be 21.5 kcal mol$^{-1}$ less exothermic than the reaction promoted by free $NO_2^+$. This value represents the BE of $NO_2^+$ to $CH_3OH$.[16] Interestingly, the CAD spectrum of the adduct **D** from the reaction in Equation (7) shows a significant $NO_2^+$ fragment, which is absent in the spectrum of the adduct **C** from the more exothermic reaction in Equation (2).[18]

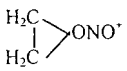


**Summary of the experimental results**: The overall picture is consistent with the hypothesis that direct nitration of acetylene by free nitronium ions is a highly exothermic process. Owing to the large excess of internal energy, the $C_2H_2NO_2^+$ ion cannot be stabilized, even at the higher pressures typical of CI experiments as compared with FT-ICR experiments. The ion undergoes complete decomposition, either by retrogression to the reactants or by dissociation into the $C_2H_2O$/NO pair, with the positive charge on either of the fragments. The nature of the fragments is such as to suggest that the adduct reaches the $H_2C{=}CO{-}NO^+$ critical configuration before undergoing dissociation. When nitration is performed with a solvated nitronium ion, $HNO_3NO_2^+$, the lower exothermicity of the process, and hence the lower internal energy excess of the $C_2H_2NO_2^+$ primary adduct, allow its partial collisional stabilization. Most of the $C_2H_2NO_2^+$ ions that survive dissociation have a structure other than $H_2C{-}C{-}O{-}NO^+$, as their CAD spectra show the presence of a strongly bonded O–N–O unit, rather than the presence of a NO unit, weakly coordinated to an O atom, as present in the $H_2C{=}CO{-}NO^+$ model ions from the nitrosation of ketene.

A similar situation prevails in the nitration of ethylene. When free $NO_2^+$ ions are involved the adduct formed, which is collisionally stabilized in this case, evolves into a species characterized as *O*-nitrosated acetaldehyde. On the other hand, when a milder nitrating agent, such as $CH_3OHNO_2^+$, is used, the adducts formed with a lower excess of internal energy retain a structure characterized by the presence of an O–N–O unit.

**Computational results**: To obtain a detailed understanding of the reaction mechanisms, the experimental results were complemented with those of a computational study. All computations reported in this paper were performed at the MP2/6–31+G* level using the Gaussian 94[19] suite of programs. These programs were chosen because they proved accurate in the study of the reaction in Equation (2).[7, 8] Furthermore, this choice allows one to compare the results for the two reactions on the same basis. All critical points were fully optimized with respect to the gradient and characterized through the computation of the analytical Hessian matrices.

The computed critical points are shown in Figures 2–5, and the corresponding energy values are reported in Table 4. The mechanistic information provided by the computed critical points is summarized in the energy profiles illustrated in Figures 6–8. We denote these reaction paths as: i) the 1,3-

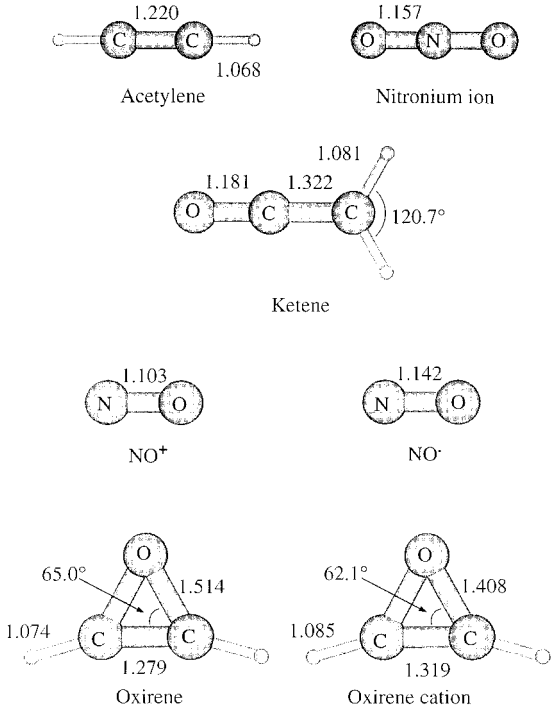


Figure 2. Optimized geometrical parameters of the reactants and products. Bond lengths are in Å and angles in degrees. The labels are the same as those used in the text.



0947-6539/00/0603-0540 $ 17.50+.50/0 *Chem. Eur. J.* **2000**, *6*, No. 3

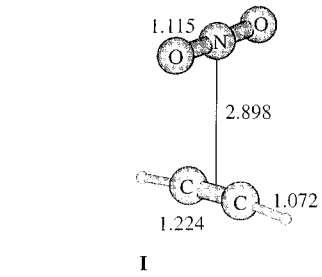


I

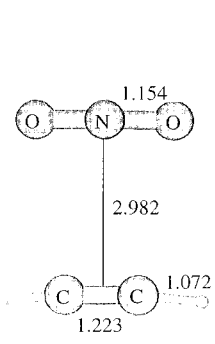


II

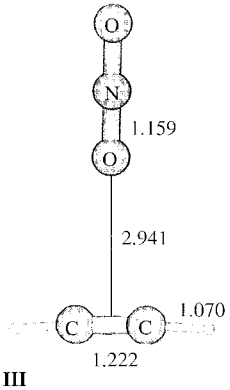


III

Figure 3. Optimized geometrical parameters of the electrostatic structures. Bond lengths are in Å and angles in degrees.

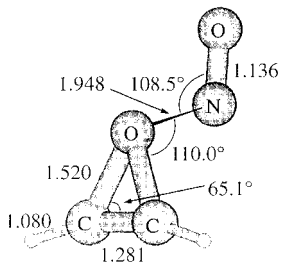


VIII

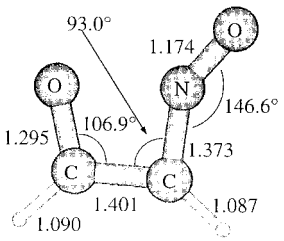


IX

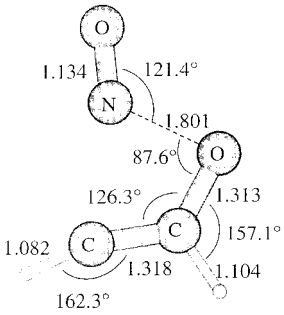


X

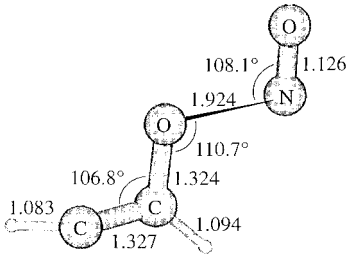


XI

Figure 5. Optimized geometrical parameters of the structures VIII, IX, X, and XI involved in the σ-type and *O*-nitroso reaction paths. Bond lengths are in Å and angles in degrees.

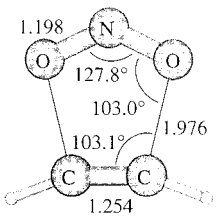


IV

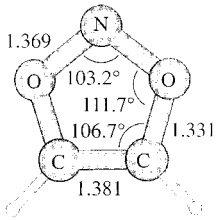


V

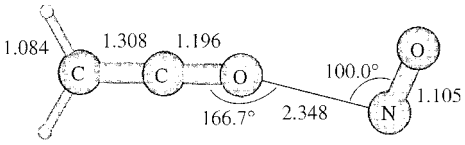


VII

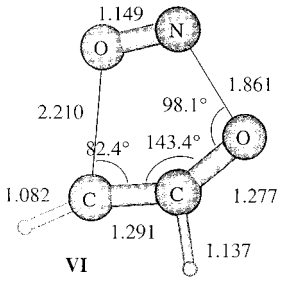


VI

Figure 4. Optimized geometrical parameters of the structures IV, V, VI, and VII involved in the 1,3-dipolar-type reaction paths. Bond lengths are in Å and angles in degrees.

dipolar-type reaction path; ii) the σ-type reaction path, which involves the σ-structure IX; and iii) the *O*-nitroso reaction path, which involves structure VIII.

We will discuss now in detail these reaction paths and we will start with the 1,3-dipolar-type reaction path. As shown in Figure 6, the reaction proceeds from the reactants and gives the electrostatic complex I, which is at an electrostatic minimum about 10 kcal mol$^{-1}$ more stable than the reactants (9 kcal mol$^{-1}$ when the zero-point energy (ZPE) corrections are included). In this region, we have also found two other critical points, denoted as structures II and III. Structure II is a transition state that connects two equivalent structures of I with a very small barrier (about 0.8 kcal mol$^{-1}$), while structure III is a second-order saddle point. Therefore, the two critical points II and III do not seem to have any significant mechanistic role. From the electrostatic minimum I, the reaction evolves through the 1,3-dipolar-type transition state (structure IV) to the 1,3-dipolar-type intermediate V and through the transition state VI to nitrosated ketene VII, which can dissociate to ketene and $NO^+$.

The main feature of this reaction profile is that the formation of the key intermediate V is highly exothermic, since this structure has a significant aromatic stabilization. Furthermore, conversion to nitrosated ketene VII and back dissociation into the reactants require almost the same energy.

We will now discuss the σ-type reaction path, which is illustrated in Figure 7. This reaction path is characterized by the minimum IX, which is significantly stabilized owing to a conjugative effect. We explored in detail the portion of the potential energy surface between the electrostatic intermediate I and structure IX, but we found only a second-order saddle point. From the minimum IX, the reaction evolves through transition state X to nitrosated ketene and then to ketene and $NO^+$.

The third reaction path, the *O*-nitroso reaction path, is illustrated in Figure 8: in this case, the system evolves, without any barriers, from the region associated with the oxygen-type

Table 4. Energies [hartrees] and relative energies [kcal mol$^{-1}$] of the reactants and of the various critical points[a] for the reaction in Equation (1).

| Critical points | | $E_h$ | $\Delta E$[c] | ZPE[d] | $E_h$ + ZPE | $\Delta(E_h$+ ZPE)[c] |
|---|---|---|---|---|---|---|
| R[b] | (M) | − 281.319604 | 0.00 | 0.035759 | − 281.283845 | 0.00 |
| I | (M) | − 281.336196 | 10.41 | 0.038091 | − 281.289105 | 8.95 |
| II | (TS) | − 281.334961 | 9.64 | 0.038075 | − 281.296886 | 8.18 |
| III | (SOSP) | − 281.329605 | 6.28 | 0.037661 | − 281.291944 | 5.08 |
| IV | (TS) | − 281.325284 | 3.56 | 0.040059 | − 281.285225 | 0.87 |
| V | (M) | − 281.432053 | 70.56 | 0.045429 | − 281.386624 | 64.49 |
| VI | (TS) | − 281.327983 | 5.26 | 0.036151 | − 281.291832 | 5.01 |
| VII | (M) | − 281.428701 | 68.46 | 0.037515 | − 281.391186 | 67.36 |
| VIII | (M) | − 281.347651 | 17.60 | 0.03732 | − 281.310331 | 16.62 |
| IX | (M) | − 281.391344 | 45.02 | 0.046046 | − 281.345298 | 38.56 |
| X | (TS) | − 281.319260 | − 0.22 | 0.36792 | − 281.292468 | − 0.86 |
| nitronium ion | (M) | − 204.246346 | | 0.010104 | − 204.236242 | |
| acetylene | (M) | − 77.073258 | | 0.025655 | − 77.047603 | |
| NO$^{\cdot}$ | (M) | − 129.566897 | | 0.008782 | − 129.558115 | |
| NO$^+$ | (M) | − 129.246978 | | 0.004814 | − 129.242164 | |
| ketene | (M) | − 152.157371 | | 0.031732 | − 152.125639 | |
| oxirene | (M) | − 152.032832 | | 0.028643 | − 152.004189 | |
| oxirene cation | (M) | − 151.730051 | | 0.033601 | − 151.696450 | |

[a] M = minimum, TS = transition state, SOSP = second-order saddle point. [b] Reactants. [c] kcal mol$^{-1}$. [d] Zero-point energy (hartrees).

attack to the minimum VIII and subsequently to nitrosated ketene (and finally to ketene and NO$^+$) through a barrier of 17.5 kcal mol$^{-1}$, or to oxirene-type products, a path that requires a significantly larger amount of energy. These three different reaction paths, i) – iii), share the important common feature that the end products are in all cases ketene and NO$^+$.

These computational results provide a sound interpretative basis for the hypothesis that direct nitration of acetylene by free nitronium ions is a highly exothermic process that yields adducts with an excess of internal energy. The excess of internal energy is sufficiently large to enable the adducts to undergo complete decomposition.

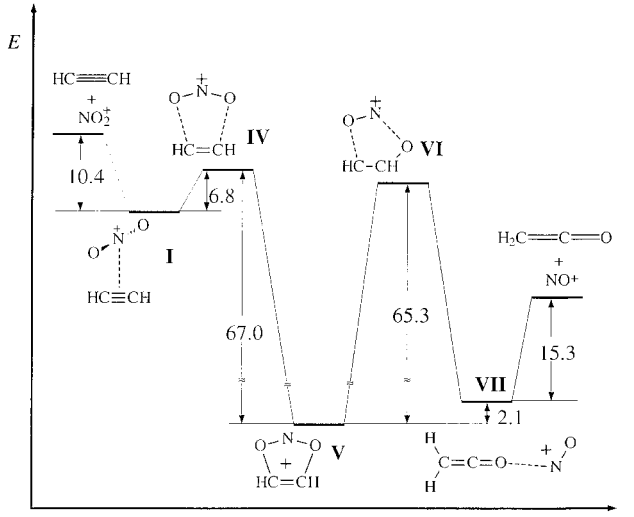


Figure 6. Energy profile of the 1,3-dipolar-type reaction path for the reaction in Equation (1).

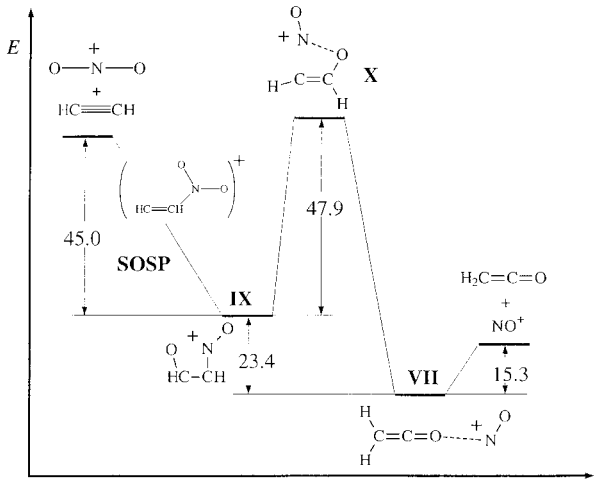


Figure 7. Energy profile of the σ-type reaction path for the reaction in Equation (1).

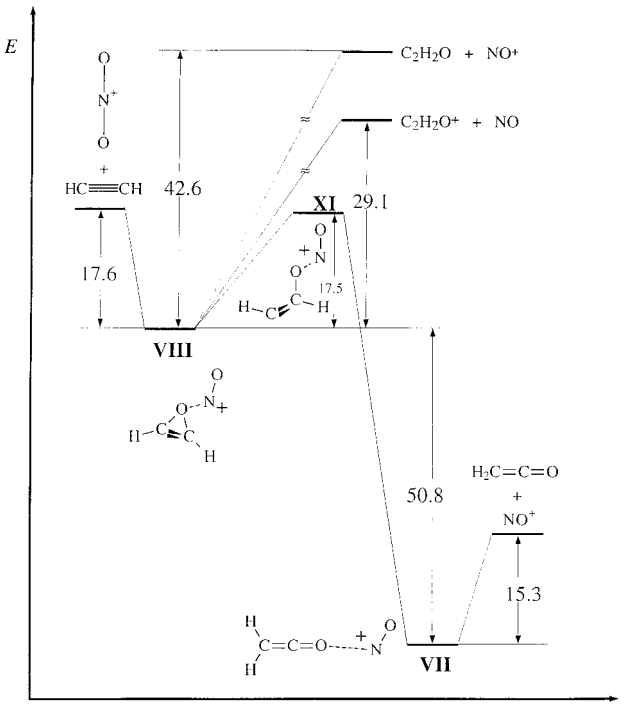


Figure 8. Energy profile of the *O*-nitroso reaction path for the reaction in Equation (1).

For comparative purposes, we will examine also the results for the nitration of ethylene by free nitronium ions that have been examined in previous studies.[7, 8] The energy profiles of the reaction paths identified are reported in Figures 9 – 11. It can be seen that the overall picture of the nitration of acetylene and ethylene by free nitronium ions is very similar. Indeed in the case of the reaction in Equation (2), three possible pathways that correspond to those of the reaction in Equation (1) were identified.



0947-6539/00/0603-0542 $ 17.50+.50/0 *Chem. Eur. J.* **2000**, *6*, No. 3

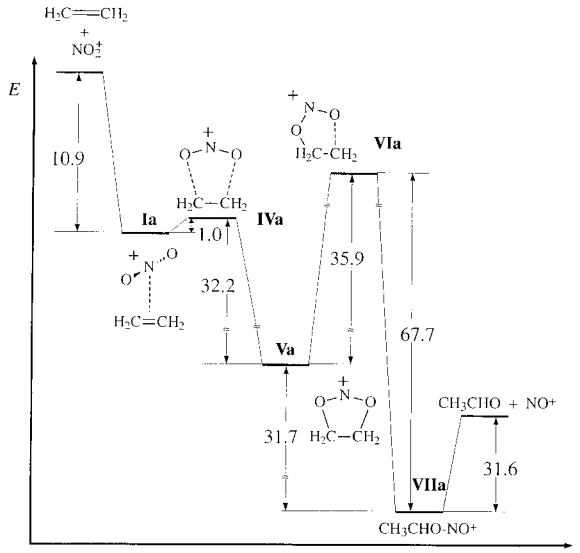


Figure 9. Energy profile of the 1,3-dipolar-type reaction path for the reaction in Equation (2). The energy of structure VIa is −282.54781 hartree.

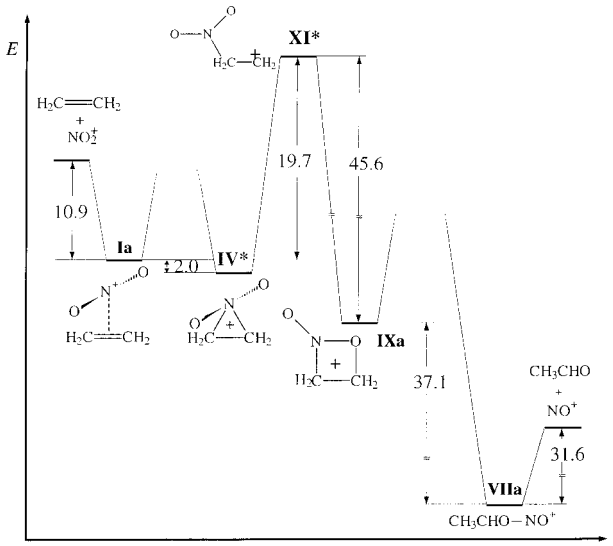


Figure 10. Energy profile of the σ-type reaction path for the reaction in Equation (2).

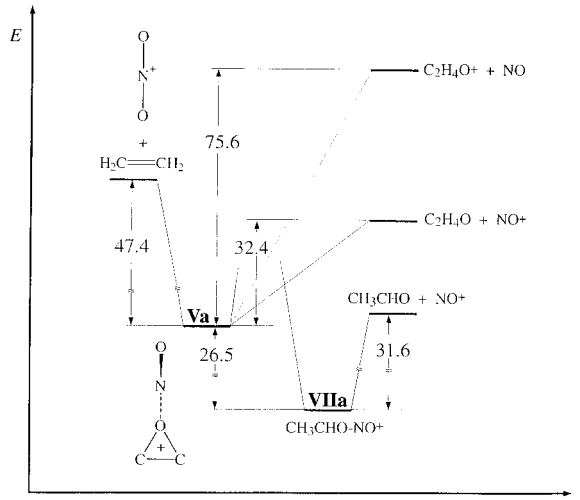


Figure 11. Energy profile of the *O*-nitroso reaction path for the reaction in Equation (2).

In Figure 9, Ia denotes the electrostatic intermediate, IVa the transition structure, and Va the intermediate found in the 1,3-dipolar-type approach. VIa denotes the transition structure, which leads to the product VIIa. In Figure 10, Ia represents the electrostatic intermediate and IXa the deep minimum. The other two critical points do not correspond to any in the reaction in Equation (1) and can be denoted as IV* and XI*. Finally, VIIa in Figure 11 denotes the *O*-nitroso form, and $C_2H_4O$ and $C_2H_4O^+$ denote oxirane and the oxirane cation.

## Discussion

The interplay of theoretical and experimental methods proved particularly fruitful in the study of the nitration of acetylene. Indeed, the theoretical picture is fully consistent with the experimental results and allows their rationalization. In turn, certain experimental features are crucial for the determination of the role of the three possible reaction pathways identified by theoretical analysis.

Consistent with theoretical predictions, the experimental evidence points to the highly exothermic character of the reaction in Equation (1). The reaction yields a nitrosated adduct with such a large excess of internal energy that its stabilization is prevented. This occurs not only in the low-pressure range typical of FT-ICR experiments, but even at the much higher pressures in the CI ion source. In all mass spectrometric experiments one observes only the reactions in Equations (3) and (4); these reactions yield the $NO^+/C_2H_2O$ and $NO/C_2H_2O^{\bullet+}$ pairs, respectively. Significantly, the $C_2H_2O^{\bullet+}$ fragment was experimentally identified as ionized ketene; this is an important clue to the mechanism of the addition–dissociation sequence. Formation of the adduct is only observed when nitration of acetylene is performed according to the reaction in Equation (5), which is less exothermic than the reaction in Equation (1) by some 20 kcal mol$^{-1}$. The dependence of the products formed on the exothermicity of the nitration process, and hence on the internal energy of the adduct, is only consistent with the 1,3-dipolar-type addition mechanism i). This is because its energy profile is the only one that displays a deep potential well, which corresponds to the particularly stable ion V. The conversion of V into the *O*-nitrosated adduct VII requires that a energy barrier as high as 65 kcal mol$^{-1}$ is overcome. This is no longer possible when the lower internal energy of ion V from the less exothermic reaction in Equation (5) is further reduced by collisional deactivation. Under these conditions, a fraction of ions V can survive, as revealed by their CAD spectra, which show the presence of a tightly bonded O–N–O unit in the species probed. The same arguments do not hold for the alternative reaction pathways, ii) and iii), whose energy profiles display relatively low barriers to conversion into VII; this would necessarily cause dissociation into ketene and $NO^+$. In summary, although mechanism i) alone would account for all major experimental features, the contribution of parallel mechanisms ii) and iii) to the formation of the ketene/$NO^+$ products cannot be ruled out.

In the case of ethylene, nitration by free $NO_2^+$ gives a $C_2H_4NO_2^+$ adduct that survives complete dissociation; this

suggests that the exothermicity of the process in Equation (2) is lower than that of the process in Equation (1). Such an inference is supported by the theoretical analysis, which shows that indeed the reaction in Equation (2) is less exothermic by some 30 kcal mol$^{-1}$ than the reaction in Equation (1). The reason for this is that the $C_2H_4NO_2^+$ adduct is not as stabilized as it lacks the aromatic character of V. A notable experimental feature is the absence of the $NO_2^+$ fragment in the CAD spectrum of the $C_2H_4NO_2^+$ ions from the reaction in Equation (2). This stands in contrast with the detection of $NO_2^+$ in the CAD spectra of the $C_2H_4NO_2^+$ ions from the reaction in Equation (7), which is less exothermic by 21.5 kcal mol$^{-1}$ than the reaction in Equation (2). Such a trend suggests that the conversion of a species with an O–N–O unit into a *O*-nitrosated species requires a sizable energy barrier to be overcome. Only ions, such as those from the reaction in Equation (2), can achieve this as they have a large excess of internal energy. The ions from the less exothermic reaction in Equation (7) are unable to cross the energy barrier, which allows survival, and hence detection, of the species with the O–N–O unit. Again, among the reaction pathways identified by the theoretical analysis the 1,3-dipolar type mechanism is consistent with the evidence from CAD spectrometry. In the first place, a species with a bridged O–N–O unit is present in the cycloaddition route, as shown by the energy profiles illustrated in Figures 9–11. Furthermore, the conversion of such a cycloaddition product into *O*-nitrosated species requires that an energy barrier as high as 35.9 kcal mol$^{-1}$ is overcome. In summary, the 1,3-dipolar-type mechanism is also the one that provides the best agreement with all the experimental features in this case. We note that $N_fR$/CA spectrometry allowed the experimental identification of the *O*-nitrosated species as nitrosated acetaldehyde, rather than nitrosated oxirane. Conventional CAD spectrometry did not allow such structural assignments, and this is consistent with the theoretical predictions (Figures 9–11). As a final remark, it is difficult to compare the present gas-phase results with those of analogous studies performed in solution. Indeed, the solution results do not fit a general pattern as in the case of aromatic nitration, and the mechanisms of the reactions with olefins or acetylenes of nitrating electrophiles can be quite different. These also depend a great deal on the specific system investigated and/or the reaction conditions.[4] Nevertheless, it is worth mentioning that the formation of cyclic ionic intermediates has been suggested in the mechanistic study of the nitration of tetrasubstituted ethylenes with nitronium salts.[20]

## Conclusion

The present results support the view that the reactions of free nitronium ions with acetylene and ethylene, the most simple aliphatic π systems, proceed according to the same mechanism, namely 1,3-dipolar cycloaddition. The major difference resides in the different stability of the cycloadduct formed, for example, the $C_2H_2NO_2^+$ ion has aromatic character and hence has more conjugative stabilization relative to the $C_2H_4NO_2^+$ ion. The thermodynamically most stable end products are in both cases *O*-nitrosated species, namely nitrosated ketene from acetylene and nitrosated acetaldehyde, rather than nitrosated oxirane from ethylene. The mechanistic picture outlined by the present work is potentially relevant to aromatic nitration by free $NO_2^+$ ions. Finally, the study underlines the usefulness of combined theoretical and experimental approaches and the considerable improvement in the structural characterization of gaseous ions made possible by $N_fR$/CA spectrometry.

## Acknowledgments

The financial support of the University of Bologna, the University of Rome "La Sapienza", MURST, and CNR is gratefully acknowledged. The authors are indebted to F. Angelelli for FT-ICR measurements.

[1] E. D. Hughes, C. K. Ingold, R. I. Reed, *J. Chem. Soc.* **1950**, 2400.
[2] G. A. Olah, *Acc. Chem. Res.* **1971**, *4*, 240.
[3] a) L. M. Stock in *Progress in Physical Organic Chemistry*, *Vol. 12* (Ed.: R. W. Taft), Wiley, New York, **1976**, Chapter 2; b) T. H. Lowry, K. S. Richardson, *Mechanism and Theory in Organic Chemistry*, 2nd ed., Harper Row, New York, **1981**, section 7.4.
[4] G. A. Olah, R. Malhotra, S. C. Narang, *Nitration: Methods and Mechanisms*, VCH, New York, **1989**.
[5] a) J. H. Ridd, *Chem. Soc. Rev.* **1991**, *20*, 149; b) L. Eberson, M. P. Hartshorn, F. Radner, *Acta Chem. Scand.* **1994**, *48*, 937.
[6] J. H. Ridd, *Acta Chem. Scand.* **1998**, *52*, 11.
[7] F. Bernardi, M. A. Robb, I. Rossi, A. Venturini, *J. Org. Chem.* **1993**, *58*, 7074.
[8] F. Cacace, G. de Petris, F. Pepi, I. Rossi, A. Venturini, *J. Am. Chem. Soc.* **1996**, *118*, 12719.
[9] G. J. Fisher, A. F. MacLean, A. W. Schnizer, *J. Org. Chem.* **1953**, *18*, 1055.
[10] P. Caravatti, M. Allemann, *Org. Mass Spectrom.* **1991**, *26*, 514.
[11] J. E. Bartmess, R. M. Georgiadis, *Vacuum* **1983**, *33*, 149.
[12] D. Thölmann, H.-Fr. Grützmacher, *ICR Ion Trap Newslett.* **1992**, *25*, 15.
[13] M. J. Polce, S. Barancova, M. J. Nold, C. Wesdemiotis, *J. Mass Spectrom.* **1996**, *31*, 1073.
[14] C. A. Schalley, G. Hornung, D. Schröder, H. Schwarz, *Chem. Soc. Rev.* **1998**, *27*, 91.
[15] J. L. Holmes, *Adv. Mass Spectrom.* **1989**, *11*, 53.
[16] a) F. Cacace, G. de Petris, F. Pepi, F. Angelelli, *Proc. Natl. Acad. Sci. USA* **1995**, *92*, 8635; b) F. Bernardi, F. Cacace, G. de Petris, F. Pepi, I. Rossi, *J. Phys. Chem.* **1998**, *102*, 1987.
[17] This is consistent with earlier mass spectrometric results that point to the structural stability of the neutral fragments of interest, see C. Wesdemiotis, B. Leyh, A. Fura, F. W. McLafferty, *J. Am. Chem. Soc.* **1990**, *112*, 8655.
[18] Unless stated otherwise, the thermochemical data are taken from a) S. G. Lias, J. E. Bartmess, J. L. Liebman, J. L. Holmes, R. D. Levin, W. G. Mallard, *J. Phys. Chem. Ref. Data Suppl.* **1988**, 17; b) E. P. L. Hunter, S. G. Lias, *J. Phys. Chem. Ref. Data* **1998**, *27*, 413.
[19] M. J. Frisch, G. W. Trucks, H. B. Schlegel, P. M. W. Gill, B. G. Johnson, M. A. Robb, J. R. Cheeseman, T. Keith, G. A. Peterson, J. A. Montgomery, K. Raghavachari, M. A. Al-Laham, V. G. Zakrzewski, J. V. Ortiz, J. B. Foresman, J. Cioslowski, B. B. Stefanov, A. Nanayakkara, M. Challacombe, C. Y. Peng, P. Y. Ayala, W. Chen, M. W. Wong, J. L. Andres, E. S. Replogle, R. Gomperts, R. L. Martin, D. J. Fox, J. S. Binkley, D. J. Defrees, J. Baker, J. J. P. Stewart, M. Head-Gordon, C. Gonzalez, J. A. Pople, *Gaussian 94* Gaussian, Pittsburgh PA, **1995**.
[20] G. A. Olah, P. Schilling, P. W. Westerman, H. C. J. Lin, *J. Am. Chem. Soc.* **1974**, *96*, 3581.

Received: June 4, 1999 [F1833]